Nano World Journal

https://doi.org/10.17756/nwj.2023-s3-133

Research Article

Open Access

Investigation on the Mechanical Properties of Dissimilar Friction Stir Welding of AA2024-AA5128 Plates with Silicon Carbide Nanoparticle Reinforcement

H.V. Ganvir[1*], K. Krishna Bhaskar[2], K. Chanthirasekaran[3], Prashant Kumar Gangwar[4], Vijay Kumar Sharma[5], Sanjay Kumar[6] and P. Satishkumar[7]

[1]*Department of Applied Physics, Yeshwantrao Chavan College of Engineering, Nagpur, Maharashtra, India*
[2]*Department of Mechanical Engineering, University College of Engineering Kakinada, JNTUK Kakinada, Andhra Pradesh, India*
[3]*Department of Electronics and Communication Engineering, Saveetha Engineering College, Chennai, Tamil Nadu, India*
[4]*Department of Construction Technology and Management, Woldia Institute of Technology, Woldia University, Woldia Town, Ethiopia*
[5]*Department of Physics, Shyam Lal College, University of Delhi, Delhi, India*
[6]*Department of Chemistry, Shyam Lal College, University of Delhi, Delhi, India*
[7]*Department of Mechanical Engineering, Rathinam Technical Campus, Coimbatore, Tamil Nadu, India*

***Correspondence to:**
H.V. Ganvir
Department of Applied Physics,
Yeshwantrao Chavan College of Engineering,
Nagpur, Maharashtra, India.
E-mail: hrwasnik@gmail.com

Received: July 31, 2023
Accepted: October 30, 2023
Published: November 01, 2023

Citation: Ganvir HV, Bhaskar KK, Chanthirasekaran K, Gangwar PK, Sharma VK, et al. 2023. Investigation on the Mechanical Properties of Dissimilar Friction Stir Welding of AA2024-AA5128 Plates with Silicon Carbide Nanoparticle Reinforcement. *NanoWorld J* 9(S3): S752-S758.

Published by United Scientific Group

Abstract

Dissimilar friction stir welding (FSW) was performed between thick slabs of aluminum alloys enhanced with silicon carbide (SiC) nanoparticles. Excellent mechanical mixing among the connected materials, uniform distribution of nanoparticles, and further grain refinement distinguish defect-free welds from their unreinforced counterparts. The generated metal matrix composites' local mechanical behavior was investigated and compared to that of the bulk and source materials. The presence of fillers is connected to the observed mechanical characteristics at the micro- and nano-scales (in particular, hardness and elastic modulus). The addition of SiC nanoparticles improves the material's mechanical properties, such as hardness, elastic modulus, ultimate tensile strength, percentage elongation, and yield value.

Keywords

Mechanical properties, Friction stir welding, Silicon carbide, Nanoparticles, Microhardness

Introduction

Solid-state joining methods like FSW have been demonstrated to produce high-quality welds in materials that previously couldn't be welded or those that were too different from one another to be welded using conventional methods. By rotating and plunging a non-consumable, cylindrical, shouldered tool with a profiled pin into the joint region between the work pieces being welded, FSW aims to fuse the metal together at the joint. Instrumental range is based on the length of the pinning mechanism below the shoulder. The strength and durability of the welds are determined by the quantity of heat input, which is managed by the tool shoulder. Porosity, inclusions, and solidification fissures are all avoided because there is no melting of the material [1].

Lightweight aluminum alloys are becoming increasingly popular due to their excellent mechanical performance in a variety of applications, including shipbuilding, transportation, and aerospace. One of the disadvantages of such alloys is that they are difficult to weld using standard techniques. The FSW of aluminum alloys has been the subject of extensive study. Authors [2] recently compared the weldability of AA5128 and AA2024 by analyzing their plastic behavior (at high temperatures).

Adhesive wear on the surface of aluminum components is quite high when

they come into touch with tougher materials, which is another drawback of using aluminum in construction. Incorporating stronger nanoparticles into the aluminum matrix is one approach to addressing this issue. Most methods for making metal matrix composites involve melting and resolidifying the metal, which has its own set of problems [3-5]. To address these concerns, friction stir processing (FSP) was created from FSW.

Improved properties may be achieved in the generated metal matrix composites by strengthening the aluminum matrices with nanoparticles [6]. Incorporating iron particles into pure aluminum-iron metal matrix composites with multipass FSP was recently reported by authors [7]. Nickel particles were incorporated into a cast aluminum A413 matrix using the FSP method by authors [8]. Different nanopowders (alumina, SiC, and boron carbide) were successfully incorporated into an AA5059 substrate by authors [9], while AA1100 was reinforced with glass, polymer, and carbon fiber attrition milled micro-powders by authors [10]. Researchers [11] looked at the inclusions that occurred in AA5052 when titanium dioxide nanoparticles were subjected to FSP. While authors [12] investigated how process conditions and particle size affected AA2024 matrix composites, utilized the same matrix to manufacture boron carbide particle surface reinforcements. To achieve surface nitriding of Ti6Al-V, the authors [13] created the friction-stir nitriding technique.

In low volume materials with a complex microstructure, conventional mechanical testing methods (such compression and tensile tests) are inappropriate for evaluating the mechanical behavior at the local level. Using a shear testing instrument optimized for use in small weld portions, the authors [14, 15] recently evaluated and sampled a number of weld zones to evaluate their plastic characteristics and shear toughness. While macroscale and microscale approaches are unable to characterize the mechanical properties of materials with very fast microstructural gradients at the local level, commercial nanoindentation equipment is able to do so because of its exceptional spatial resolution [16].

FSWed-like aluminum alloys have been studied earlier for their nanomechanical behavior and residual stress distribution. The addition of reinforcing particles to an FSW is another topic of study [17]. Continuous research of dissimilar welds by exploring SiC's impact as a reinforcing material in AA2024-H111 and AA5128-T6 was carried out. Since there is an additional parameter being probed, a different approach has been adopted, and the scope of the experimental effort has substantially increased. Symbols in each test denote whether the AA2024-H111 is on the leading edge or the trailing edge, representing the new variable that is the direction of the passes. According to the findings, the stir zone nanoparticle dispersion may be influenced by the number and orientation of FSP passes. The goal of this research is to analyze the mechanical properties of welded joints made by utilizing a friction stir butt technique to join plates of AA2024-H111 and AA5128-T6 with SiC fillers. The low electrical and strong chemical conductivity of SiC, together with its inexpensive cost and simplicity of manufacture, made it an attractive material. Mechanical qualities of the best welds were tested using microhardness measures, tensile testing, and nanoindentation to determine their excellence.

Materials and Method

Extruded plates of AA5128 are used to make the major stiffener panels of high-speed aluminum alloy ships in the maritime sector. The ship's hull, built of corrosion resistant AA2024 was reinforced with these stiffeners. As a result, the ship's hull's primary stiffener panels and secondary stiffener panels have different welds. FSW can also be used to mass-produce primary stiffener panels. High welding temperatures, especially in the heat affected zone (HAZ), degrade the mechanical characteristics of precipitation hardened materials like AA5128 in the T6 state. To reduce this impact, a metal matrix composite can be created at the weld line by adding SiC nanoparticles. Chemical vapor deposition was used to create SiC nanoparticles. The nanoparticles appear to be spherical, with radii of around 150 - 200 nm.

The welding was done in a direction that was perpendicular to the rolling of the plates. Half grooves were cut into the contacting surfaces of the plates to accommodate the nanoparticles. A groove of 180 mm in length, 1mm in width, and 2.5 mm in depth was created when the plates were securely clamped together. After being made more controllable by adding ethanol, the SiC nanoparticles were pushed firmly into the groove. The pin's groove coincided with its central axis as it rotated. In accordance, equation 1 predicts that 13.8% of the nanoparticles' total volume will be in the stir zone.

$$V_f = \frac{\text{Area of groove}}{\text{Projected area of tool pin}} \text{ x } 100 \quad (1)$$

In order to determine the best welding settings between base metals, the scientists first ran a trial without adding SiC. Table 1 displays the results of experimenting with several values for the traverse speed (70 - 90 mm/min), rotational speed (800 - 1600 rpm), and tool tilt angle (0.0 - 4.0°). For the sake of comparison, this Sample was also used to examine how the dispersion of nanoparticles affected mechanical behavior.

The optimal welding parameters for the specimens without the inclusion of SiC nanoparticles were determined first, and then the equivalent ones for the specimens with the addition of nanoparticles were developed. All of the tests (with nanoparticle addition) made use of the same apparatus as the

Table 1: FSW experimental factors.

Sample code	Rotational speed (rpm)	Number of passes (mm)	Direction of passes
S1	800	3	AAA
S2	1200	2	AA
S3	1200	3	AAA
S4	800	2	AR
S5	800	3	ARA
S6	1600	3	ARA
S7	1200	3	ARA
S8	1600	3	AR
S9 (without SiC)	800	1	A

best one (without nanoparticle addition), a cylinder with a left-hand threaded pin measuring 3.3 mm in height and 8 mm in diameter. The round diameter of the tool's flat shoulder was 24 mm. This was because the material flow generated by this particular pin led to excellent material mixing. Weld pitch can be adjusted simply by changing the rotational speed; thus, we didn't change anything else but that. The transverse speed was kept at 90 mm/min, tool tilt angle was at 2°, and tool pin penetration depth was at 2.50 mm. Finally, the direction and number of FSP passes are reported to alter the dispersion of SiC particles in the stir zone. Because of this, the authors opted to apply the Taguchi technique to determine the best settings for the welding tests. Taguchi analysis revealed that conducting mechanical testing required just 8 out of a possible L8 orthogonal array of trials. The results of these analyses are shown in table 1.

In each experiment, the letters A and R denote whether the AA2024-H111 is progressing forward or falling behind. A tool with a 24 mm diameter shoulder and no pin is used to pass the SiC particles through the grooves once, preventing them from being expelled during the FSW process. Covering was rotated at 800 rpm, shifted at 90 mm/min transversely, and slanted at 2° in all tests. A Kistler piezo-multicomponent dynamometer was used to measure the axial load with a force-controlled method. Once the instrument was set into the metal matrix, the force was maintained at around 10 kN.

The longitudinal microhardness (Vickers) distributions of the samples were measured using a Wolpert Wilson 402MVD microhardness tester. There was a 300 g force exerted. Longitudinally along two lines 2 mm and 4 mm below the surface, microhardness readings were taken. In accordance with the ASTM E 8M-04 standard, tensile specimens were forged = shaped in a direction orthogonal to the welding direction. The MTS 100 kN maximum load hydraulic mechanical testing equipment was utilized for the tensile tests. An Epsilon 25 mm extensometer was used to determine the length. It was stretching at a rate of 0.5 mm/min.

The diamond indenter used for the nanoindentation tests was shaped like a Berkovich pyramid. At a range of maximum indentation depths, loading times of 40 sec, 3 sec of holding time, and 40 sec of emptying segment time were employed in the loading control mode. The welds' cross-sections were used for the nanoindentation measurements, which were performed 4 mm below the welding substrate in both directions.

Nanoindentation involves penetrating a material's surface with a known-geometry indenter while simultaneously monitoring the load and depth of the indentation. Nanoindentation hardness may be determined using equation 2.

$$H = \frac{P_{\max}}{A(h_c)} \tag{2}$$

Where '$A_{(hc)}$' is the region of the Berkovich indenter's projected contact with the material and 'P_{max}' is load determined by the deepest point of indentation (h_{max}).

To express $A_{(hc)}$ as a function of the contact indentation depth hc,

$$A(h_c) = 24,5h_c^2 + a_1h_c + a_{1/2}h_c^{1/2} + \ldots + a_{1/16}h_c^{1/16}$$

$$h_c = h_{\max} - \varepsilon\frac{P_{\max}}{s} \tag{3}$$

Where ε = 0.75 and

$$S = \left(\frac{dP}{dh}\right)h = h_{\max} \tag{4}$$

Results and Discussion

Each specimen's stir zone grain size was compared to that of S without nanoparticle addition and the base materials (Table 2). Processing results in smaller grains because of dynamic recrystallization. The SiC nanoparticles acted as pins in the stir zone, preventing grain expansion during dynamic recrystallization, resulting in smaller grains than in the unreinforced specimen.

Table 2: Particle grain size.

Sample	Size of grain (μm)
AA5128	45
AA2024	32
S9	15
S3	4
S6	4

Figure 1 shows a comparison between the longitudinal microhardness distribution of the weld 4 mm distant from the shoulder surface and the weld with nanoparticle addition. Although the nanoparticle-containing sample was unstable in the stir zone, its average microhardness of 13 HV0.3 was 18% greater than that of the unreinforced sample and higher than that of the AA2024-H111 base material. Since hardness decreases as grain size increases, this fits well with the Hall-Petch relation. Table 2 shows particles in the particle-free zone were much larger than those in the reinforced stir zone. When compared to the other retarding sides, the AA5128-T6 (HAZ region) side has the softest microhardness at 52 HV0.3 or less. Although AA5128 may be heat treated, its T6 state is

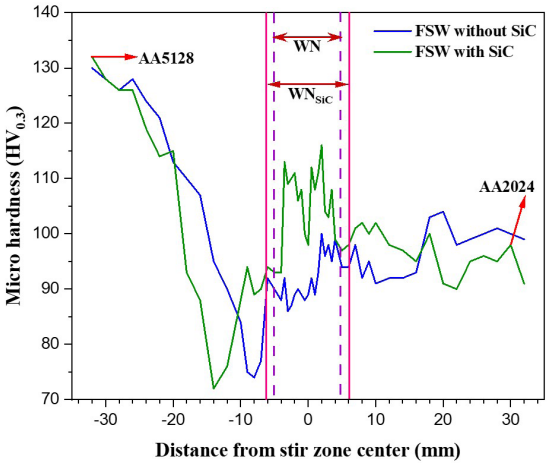

Figure 1: Microhardness profile of the without SiC and with SiC reinforced joints.

precipitation hardened, and FSW dissolves the strengthening precipitates. Microhardness testing also shows that HAZ hardness values rise towards the direction of the stir zone. This is because new precipitates are stimulated = accelerated by the increased temperatures that occur close to the stir zone.

AA2024-H111 parent material has a Hmicro mean average of 80 HV0.3, while AA5128-T6's had 105 HV0.3. While AA2024 is in a strain hardened H111 condition, the parent alloy AA5128-T6 state. This is supported by the observed Hmicro distribution throughout the whole sample length (Figure 2).

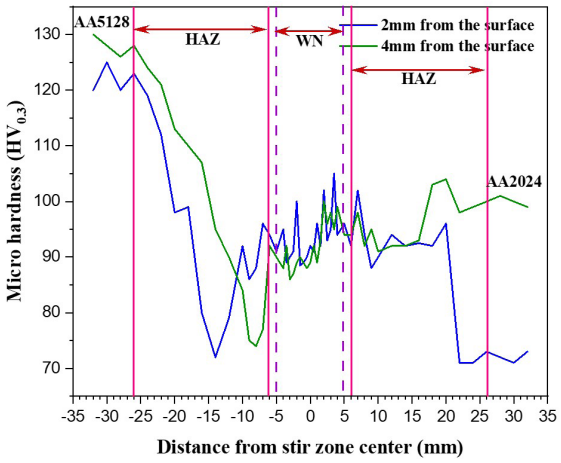

Figure 2: Microhardness profile of the SiC strengthened joint (S3).

For S3, measurements of longitudinal microhardness (Hmicro) were taken at 4 and 2 mm from the shoulder surface. Higher values in the microhardness distribution may be seen at a distance of 2 mm because the flow arm reaches into the stir zone. The flow arm has fewer nanoparticles and is a finer grain size. On the AA5128-T6 side, the HAZ values are lower at 2 mm from the shoulder surface because of the additional annealing that occurs there.

Microhardness measurements taken 4 mm from the shoulder surface reveal interesting differences between nanoparticle-added S6 and nanoparticle-free weld (Figure 3). The results are similar to those of S3, but with typically lower microhardness values in the stir zone. The S is in the stir zone achieves the same microhardness as the comparable AA2024-H111 base material and is almost 8 HV0.3 harder than the unreinforced S is (10% harder).

Figure 4 displays the results of S6 longitudinal microhardness (Hmicro) measurements taken at 4 and 2 mm from the shoulder surface. Weld nugget microhardness distribution shows reduced variance at 4 mm distance from shoulder surface compared to the distribution at 2 mm distance from shoulder surface. However, the mean value of the microhardness in the stirring zone remains almost the same regardless of the distance from the shoulder surface. All other zones show outcomes that are in line with S3 (HAZ, TMAZ).

The hardness distributions in the stir zone were statistically indistinguishable from the distributions in the parent

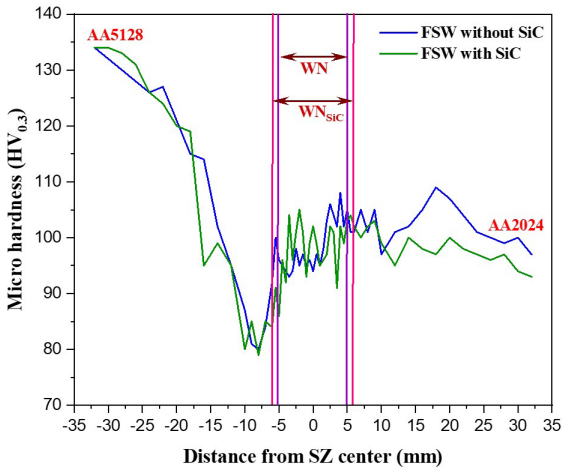

Figure 3: Microhardness welds, with and without SiC at 4 mm beneath the surface.

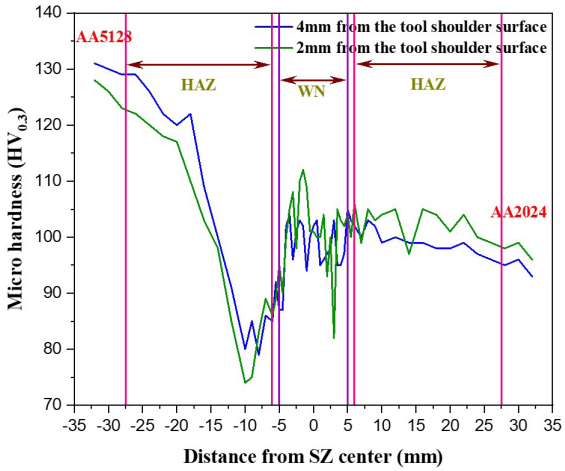

Figure 4: Microhardness weld with SiC nanoparticles (S6).

material, AA2024-H111. HAZ on AA5128-T6 side, where strengthening precipitates had dissolved, had the lowest values, as reported in the relevant literature [16]. Because the T6 heat treatment is lost during welding, the material's mechanical strength drops, as measured by Hmicro. In AA5128 alloy, the precipitates "Mg5Si6, which is stable below 300 °C, play a crucial role as a reinforcing agent". The β" is dissolved at weld temperatures greater than 250 °C. The production of β" is encouraged in HAZ, where temperatures average about 300 °C, whereas in stir zone, temperatures are greater, leading to the dissolution of Mg-Si precipitates. Small amounts of the β" precipitates are produced in stir zone during cooling. HAZ has greater Hmicro values than TMAZ because of the presence of β. The dynamic recrystallization process results in a very fine grain structure, which is reflected in the nugget's Hmicro recovery.

Tensile tests were performed on both S3 and S6, despite the fact that S3 had higher microhardness values in the stirring zone. Percentage elongation, Young's modulus, universal tensile strength (UTS), and yield stress are shown in table 3 as averages (based on three tests) for S3. The relationship between stress and strain for reinforced and unreinforced SiC

Table 3: Weld mechanical characteristics (mean values) with and without SiC nanoparticle addition.

Sample	Young's modulus (GPa)	Yield stress (MPa)	UTS (MPa)	Elongation (%)
S3	76.8	1452	1993	3.70.3
S6	75.4	1403	1794	1.30.2
S9	66.2	1403	1935	30.4

samples is shown in figure 5. Figure 6 displays tensile curves for the elastic deformation area of the samples; all of the aforementioned metrics show considerable increases owing to the SiC reinforcement, most notably Young's modulus (stress below yield point). The lack of improvement was traced to the start of plastic deformation and fracture in the HAZ, which does not include nanoparticles. More investigation into the precise mechanism responsible for this trend is warranted. All of the broken test pieces were located in AA5128's HAZ. The failure of the specimens beyond the stir zone reflects the strong adherence of the SiC particles to the metal matrix and the fine nanoparticle scattering in the stir zone.

However, S6 was unsuccessful in the stir region. Since S3 and the observed Young's modulus and yield stress both exhibit comparable elastic behavior, the two values are almost identical. The yield stress is lower than S3's but still close to that of the unreinforced specimen. The S3 and unreinforced sample equivalents are both higher than the UTS. Tensile test results for samples 3 and 6 are compared to one another in figure 7.

Nanoindentation was used to evaluate the nano-hardness and elastic modulus of each weld zone, and the local deformation mechanism of the SiC reinforced dissimilar metal matrix composite in the stir zone was studied. The intersection of the two parent materials (the "weld zone cross section") was the site of the experiments. As shown in figure 8, the average nano-hardness (Hnano) values were found to be lower than those of base metals. In addition, it was found that the dissolution of the precipitates led to lower nano-hardness values in the HAZ, next to AA5128-T6. However, it was discovered that the inclusion of reinforcement SiC particles increased the WN's nano-hardness.

Measured in the transverse direction at the stir zone's midpoint between the shoulder and anvil surfaces, microhardness and nano-hardness values are reported for both reinforced and unreinforced joints. Figure 9 shows that the distributions of microhardness and nano-hardness follow a very similar pattern. However, when looking at the nano hardness distribution, it is clear that the stir zone has greater hardness values than the other weld zones. Weld Hmicro was enhanced by the use of fillers, leading to a more even distribution of Hmicro in the longitudinal and transverse directions.

Nanoindentation measurements of elastic modulus are reduced after the welding procedure (in the side of AA5128-T6). When SiC nanoparticles were included, however, the values were shown to rise in the stir zone.

Tensile testing was used to evaluate Young's modulus of bone-like materials reinforced and unreinforced SiC

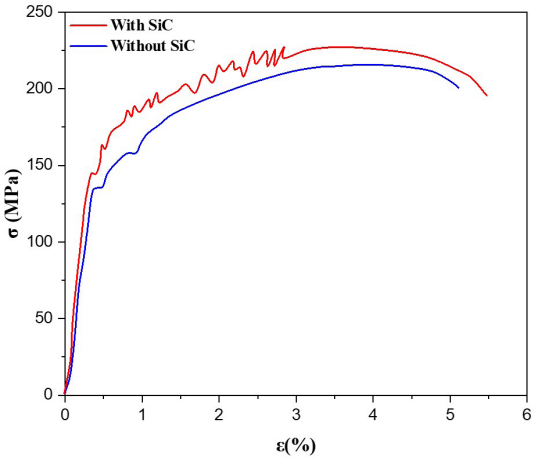

Figure 5: Stress vs Strain curvature of tensile tests of the FSW joints.

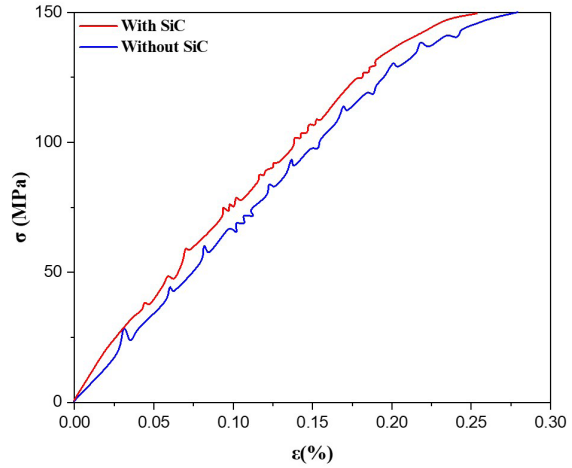

Figure 6: Stress vs Strain curvature at the elastic zone.

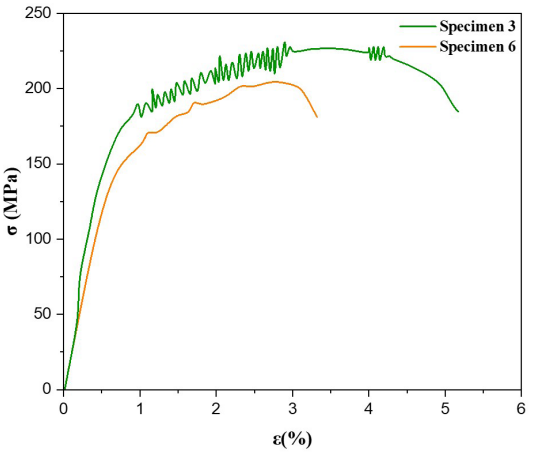

Figure 7: Evaluation of the Stress vs Strain curvatures tested at S3 and S6 samples.

nanoparticles, and the findings are shown as lines of best fit in figure 10. Local (nanoindentation measurements) and global (tensile) improvements in elastic modulus following the incorporation of SiC nanoparticles are demonstrated. Aluminum alloys and composite joints' mechanical strength may be characterized with microhardness, nano-hardness, and

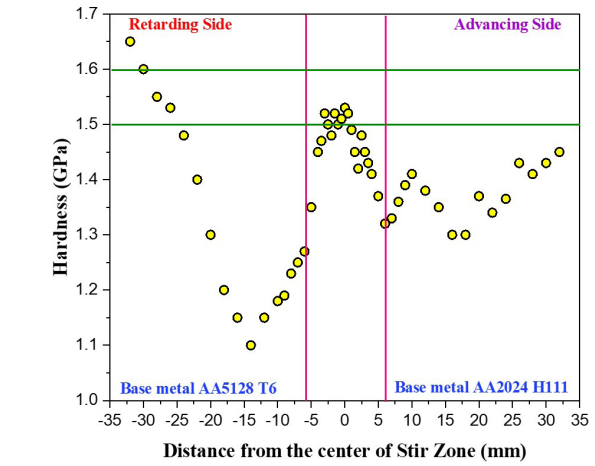

Figure 8: Nano-hardness profile of the SiC reinforced joints.

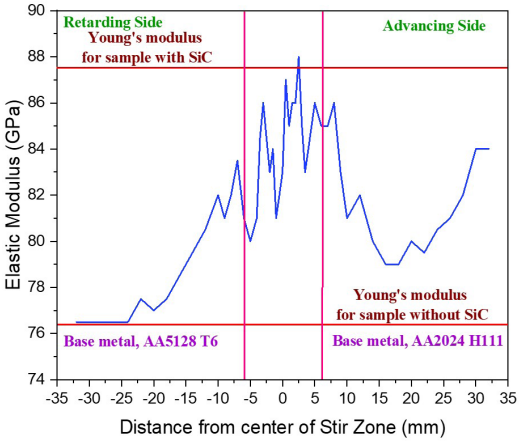

Figure 10: The elastic modulus distribution throughout the length of the joints strengthened with SiC.

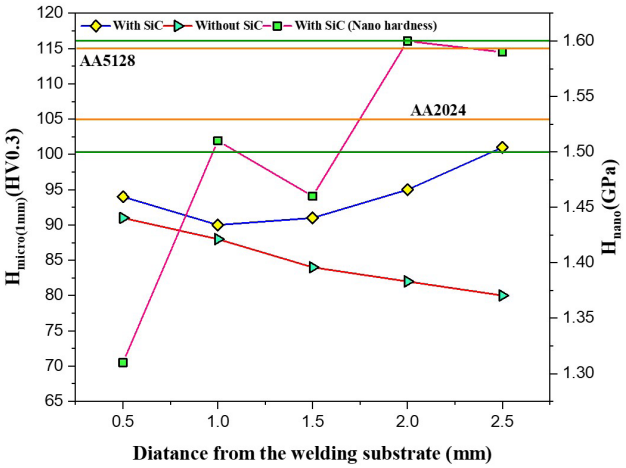

Figure 9: Transversal microhardness with and without SiC.

elastic modulus studies using indentation testing (with SiC particles). The presence or absence of reinforcing particles, as well as the grain size and dislocation density, may be inferred from the measured quantities. As was previously noted, particle size has a direct correlation with hardness [13]. Aside from the inherent hardness of reinforcing particles, the action of SiC particulates in pinning grain boundaries also contributes to the material's hardness.

Conclusions

The purpose of this study was to examine the effects of adding SiC nanoparticles to aluminum alloys in the H111 and T6 conditions to see which was more beneficial for enhancing FSW. The nano (indentation), macro (tensile) and micro (hardness) mechanical features of the produced joint were studied after optimal parameter setup, and the results were as follows:

Three FSP runs at 1600 rpm and 90 mm/min in the transverse direction resulted in the most even dispersion of nanoparticles. While there was some clumping of SiC nanoparticles in the stir zone near the flow arm region, overall, the dispersion of nanoparticles was rather equal.

- When compared to an unreinforced specimen, the microhardness of the stir zone rose by 18% when SiC nanoparticles were added. The microhardness was lowest in the HAZ of the heat-treated material and distributed similarly to other FSP samples outside of it (AA5128-T6).
- The HAZ of AA5128 correlates to the material's lowest hardness, as revealed by the tensile tests. This indicates that the stir zone was effective in distributing the particles and ensuring that the SiC particles bonded to the metal matrix. Nanoparticle incorporation also led to slight enhancements in Young's modulus, yield stress, UTS, and elongation at break.

Acknowledgements

None.

Conflict of Interest

None.

References

1. Ramachandran KK, Murugan N, Kumar SS. 2015. Friction stir welding of aluminum alloy AA5052 and HSLA steel. *Weld J* 94(9): 291s-300s.
2. Andrade DG, Leitão C, Dialami N, Chiumenti M, Rodrigues DM. 2020. Modelling torque and temperature in friction stir welding of aluminium alloys. *Int J Mech Sci* 182: 105725. https://doi.org/10.1016/j.ijmecsci.2020.105725
3. Yürük A, Ayan Y, Cevik B, Kahraman N. 2021. Investigation of mechanical and microstructural properties of AA5754/AA6013 dissimilar aluminium alloys joined by GMAW and FSW methods. *Metall Mater* 59(4): 245-256.
4. Majeed T, Mehta Y, Siddiquee AN. 2022. Al alloy tailor welded blank fabrication by friction stir welding: effect of double-pass. *J Mater Eng Perform* 31(1): 410-423. https://doi.org/10.1007/s11665-021-06161-w
5. Ahmed MM, El-Sayed Seleman MM, Zidan ZA, Ramadan RM, Ataya S, et al. 2021. Microstructure and mechanical properties of dissimilar friction stir welded AA2024-T4/AA7075-T6 T-butt joints. *Metals* 11(1): 128. https://doi.org/10.3390/met11010128
6. Kumar KSA, Murigendrappa SM, Kumar H. 2019. Experimental investigation on effects of varying volume fractions of SiC nanoparticle reinforcement on microstructure and mechanical properties in friction-stir-welded dissimilar joints of AA2024-T351 and AA7075-T651. *J Mater Res* 34(7): 1229-1247. https://doi.org/10.1557/jmr.2018.445

7. Mohapatra DK, Mohanty PP. 2023. Parametric Studies of Dissimilar Friction Stir Welded AA2024/AA6082 Aluminium Alloys. In Pradhan P, Pattanayak B, Das HC, Mahanta P (eds) Recent Advances in Mechanical Engineering. Lecture Notes in Mechanical Engineering. Springer, Singapore, pp 191-200.
8. Masoumi Khalilabad M, Zedan Y, Texier D, Jahazi M, Bocher P. 2022. Effect of heat treatments on microstructural and mechanical characteristics of dissimilar friction stir welded 2198/2024 aluminum alloys. *J Adhes Sci Technol* 36(3): 221-239. https://doi.org/10.1080/01694243.2021.1917868
9. Muruganandam D, Raguraman D, Kumaraswamidhas LA. 2019. Effect of process parameters in friction stir welding of dissimilar aluminium alloys. *IOP Conf Ser Mater Sci Eng* 574: 012009. https://doi.org/10.1088/1757-899X/574/1/012009
10. Kumar KS, Devaraju A, Manichandra B. 2020. Investigating the mechanical and metallographic properties of FSWed dissimilar 6061 & 2024 aluminum alloys by varying distinctive parameters. *Mater Today Proc* 24: 880-886. https://doi.org/10.1016/j.matpr.2020.04.398
11. Sun Z, Yang X, Liu K. 2019. Study of technology and structure property on friction plug welding of dissimilar aluminum alloy. *Trans China Weld Inst* 40(9): 145-150.
12. Robe H, Zedan Y, Chen J, Monajati H, Feulvarch E, et al. 2015. Microstructural and mechanical characterization of a dissimilar friction stir welded butt joint made of AA2024-T3 and AA2198-T3. *Mater Charact* 110: 242-251. https://doi.org/10.1016/j.matchar.2015.10.029
13. Moradi MM, Aval HJ, Jamaati R. 2017. Effect of pre and post welding heat treatment in SiC-fortified dissimilar AA6061-AA2024 FSW butt joint. *J Manuf Process* 30: 97-105. https://doi.org/10.1016/j.jmapro.2017.08.014
14. Moradi MM, Jamshidi Aval H, Jamaati R. 2018. Microstructure and mechanical properties in nano and microscale SiC-included dissimilar friction stir welding of AA6061-AA2024. *Mater Sci Technol* 34(4): 388-401. https://doi.org/10.1080/02670836.2017.1393976
15. Song X, Feng X, Zhao H, Guo L. 2015. Microstructure and mechanical properties of dissimilar barrier butt joints of AA6061/SiC/55p to AA2024 in friction stir welding. *Trans China Weld Inst* 36(11): 73-76.
16. Bagheri B, Alizadeh M, Mirsalehi SE, Shamsipur A, Abdollahzadeh A. 2022. Nanoparticles addition in AA2024 aluminum/pure copper plate: FSSW approach, microstructure evolution, texture study, and mechanical properties. *JOM* 74(11): 4420-4433. https://doi.org/10.1007/s11837-022-05481-z
17. Morales C, Merlin M, Fortini A, Garagnani GL, Miranda A. 2022. Impact behaviour of dissimilar AA2024-T351/7075-T651 FSWed butt-joints: effects of Al_2O_3-SiC particles addition. *Fract Struct Integr* 16(60): 504-515. https://doi.org/10.3221/IGF-ESIS.60.34